JOURNAL OF COMPUTATIONAL PHYSICS 98, 269–284 (1992)

A Numerical Method for Solving Systems of Linear Ordinary Differential Equations with Rapidly Oscillating Solutions

IRA B. BERNSTEIN*,†, LEIGH BROOKSHAW*,‡ AND PETER A. FOX†

* *Department of Applied Physics, Yale University, Yale Station, New Haven, Connecticut 06520-2159; and*
† *Center for Solar and Space Research, Yale University, P.O. Box 6666, New Haven, Connecticut 06511-6666*

Received October 20, 1989; accepted July 20, 1990

A numerical method is presented which allows the accurate and efficient solution of systems of linear equations of the form $dz_i(x)/dx = \sum_{j=1}^{N} A_{ij}(x)\, z_j(x)$, $i = 1, 2, ..., N$, when the solutions vary rapidly compared with the $A_{ij}(x)$. The method consists of numerically developing a set of basis solutions characterized by new dependent variables which are slowly varying. These solutions can be accurately computed with an overhead that is substantially independent of the smallness of the scale length characterizing the solutions. Examples are given.

1. INTRODUCTION

Many problems in physics and astronomy involve the solution of sets of linear ordinary differential equations $dz_i(x)/dx = \sum_{j=1}^{N} A_{ij}(x)\, z_j(x)$, $i = 1, 2, ..., N$, the solutions $z_i(x)$ of which exhibit variation on a local scalelength much less than that characterizing the coefficients $A_{ij}(x)$. Examples are to be found in the propagation of electromagnetic waves, in the theory of microwave devices such as free electron lasers [1], in control theory [2–4], in terrestrial seismology [5], and in the theory of stellar pulsations [6]. Often the coefficients $A_{ij}(x)$ are not given analytically, but numerically.

The most often used approximate method, the WKB technique [7] is simple only for the case $N \leqslant 2$ and when the coefficients are analytic (we will not discuss general perturbation methods for which the reader is referred to Kevorkian [8] and references therein). For systems of higher order, the usual method of solution is direct numerical integration of the problem using a standard package (e.g., an adaptive Runge–Kutta technique [9]). This approach has a number of drawbacks. If high accuracy is required then ~ 50 points per local characteristic length of the solution must be taken to achieve ~ 4-figure accuracy and the computational overhead goes up roughly linearly with the number of oscillations. Moreover, to generate many solutions as may be necessary if the problem involves an eigenvalue and if many of these and the associated eigenfunctions are required, and these results are to be used to compute normalization and other integrals, the task of storing the results or computing the required functions (while integrating) is usually prohibitive. In this paper we present a method which does not suffer from many of the aforementioned disadvantages. It involves a computational overhead which is substantially independent of the local wavelength and presents the solution in terms of quantities which vary on the intrinsic scalelength of the coefficient matrix $A_{ij}(x)$ and hence can be much more easily stored for other purposes.

The technique [20] is motivated by the WKB method, but can be used to numerically compute solutions to any desired degree of accuracy. The process involves the numerical development of a linearly independent set of solutions of the governing system of differential equations which span the solution space. They have the form of asymptotic solutions appropriate to the short local scale length limit plus remainder. Schematically one generates, numerically, N solutions of the form $z_s(x) = b_s(x) \exp \int k_s(x)\, dx$, $s = 1, 2, ..., N$, where the $k_s(x)$ are the eigenvalues of the matrix $A_{ij}(x)$. It is assumed that some or all of the $k_s(x)$ are large and well separated but slowly varying, and they account for the dominant rapid variation in $z_s(x)$. The amplitudes $b_s(x)$ which we calculate are of order unity and slowly varying, apart from a fluctuating part which is asymptotically small as the number of oscillations or e-folding rate grows. Usually this remainder can be either neglected or calculated with low precision.

In some problems the rapidly varying solutions may change character from rapidly growing to rapidly oscillating. The thin regions in x which separate the larger subdomains where a given asymptotic behavior prevails are most conveniently dealt with by reversion to solution of the original equations. This feature, the counterpart of dealing with a boundary layer in an asymptotic analysis, does not

‡ Now at IGPP/LLNL, L-413, P.O. Box 808, Livermore, CA 94550.

0021-9991/92 $3.00

materially diminish the efficiency of the method. A procedure for estimating the effective width of this boundary layer, which has worked well in all the test cases to be described, is given in the Appendix.

The theory of the method is given in Section 2. It is first motivated by considering the case where the $A_{ij}(x)$ are constant. This suggests the form of the solution for the case of the $A_{ij}(x)$ slowly varying on the scalelength of the solution and indicates a plausible analytic perturbation theory, a generalization of the WKB method which formally can be carried to arbitrary order. Then a numerically convenient scheme based on the analysis is presented.

In Section 3 the method is applied to a second-order differential equation ($N=2$) for which an exact solution in terms of Bessel functions is available. It was chosen in order to develop and prove the numerical implementation, to determine the accuracy at each stage of the calculation, and to test the sensitivity of the method to various parameters. The method is shown to work very well indeed. It easily copes with both oscillating and exponentially growing solutions. One verifies that the computational overhead is independent of the number of nodes in the solution, this being accomplished with the same fixed number of grid points for all cases.

In Section 4 the method is applied to the problem of calculating eigenfrequencies and eigenmodes for the non-radial oscillations in stars. This eigenvalue problem is described by a fourth-order system of ordinary differential equations. The spectrum of eigenvalues has effectively two branches, one infinite set which goes to infinity, and another infinite set which condenses on zero. The system can be approximately reduced to a second-order system for very large or very small eigenvalues. The results of the method presented here were compared with those obtained by a shooting technique employing a Runge–Kutta integrator. Both methods produced accurate results, but the time for the new method was substantially constant, while that for the other increased with the number of oscillations in the solution. This example also demonstrated that the new method could be used to determine those solutions regular at the singular point at the origin, without recourse to a series solution. The special features of the new method will permit the rapid economical investigation of the effect of changing boundary conditions on the modes, will allow the easy determination of the asymptotic spacing of eigenvalues and the ready computation of normalization and other integrals such as enter non-linear theories of weak stellar turbulence. Finally, Section 5 summarizes the work.

Appendix A shows how to reduce and solve the boundary layer problem that enters in the thin region straddling the point where two eigenvalues $k_s(x)$ coalesce and which separates the rapidly growing and rapidly oscillating subdomains. The result is an approximate local solution in terms of Airy functions which allows an approximate asymptotic matching of regions. For the purpose of this work the important result is an expression for the effective width of the thin region in terms of easily computed properties of the matrix $A_{ij}(x)$.

2. THEORY FOR A SYSTEM OF ORDINARY DIFFERENTIAL EQUATIONS

2.1. *Theory*

In this section we will develop the transformation of a general system of linear ordinary differential equations which leads to the basis set of solutions employed for the numerical work. The procedure is suggested by what happens when the coefficients in the system are constant. In general, regions where the aforementioned procedure is valid are separated by domains, often thin boundary layers, in which it fails. The joining of such regions is treated last in the section.

Consider the following system of linear, ordinary differential equations

$$\frac{d\mathbf{z}(x)}{dx} = \mathbf{A}(x)\,\mathbf{z}(x), \tag{1}$$

where $\mathbf{z}(x)$ denotes the column vector with elements $z_1(x)$, $z_2(x)$, $z_3(x)$, ..., $z_{N-1}(x)$, $z_N(x)$ and the square matrix $\mathbf{A}(x)=[A_{ij}(x)]$, $i,j=1, 2, ..., N$. Define eigenvectors $\mathbf{e}_j(x)$ and eigenvalues $k_j(x)$ of $\mathbf{A}(x)$ via $\mathbf{A}\mathbf{e}_j = k_j\mathbf{e}_j$. Then the k_j are the roots of the characteristic equation $\det|\mathbf{A}-k\mathbf{I}|=0$. Suppose that the eigenvalues $k_j(x)$ are all distinct in the interval in x of interest. Then the associated eigenvectors are linearly independent [10]. Let $\mathbf{E}(x)$ be a matrix whose columns are the eigenvectors $\mathbf{e}_j(x)$. It follows that $\det\mathbf{E}\neq 0$ and the inverse $\mathbf{E}^{-1}=\text{adj}\,\mathbf{E}/\det\mathbf{E}$ exists. It is readily seen that $\mathbf{E}^{-1}\mathbf{A}\mathbf{E}=\mathbf{K}=[k_j\delta_{ij}]$.

The desired set of basis solutions is constructed as follows. Introduce a column vector $\mathbf{b}_s(x)$ and a characteristic exponent $\int_{x_0}^{x} k_s(x')\,dx'$, using

$$\mathbf{z}_s = \mathbf{E}\mathbf{b}_s \exp\left[\int_{x_0}^{x} k_s(x')\,dx'\right], \tag{2}$$

where x_0 is a reference (normalization) point chosen for convenience and s represents the index labeling one of the linearly independent solutions of (1). The governing equation (1) becomes

$$\frac{d}{dx}\left\{\mathbf{E}\mathbf{b}_s \exp\left[\int_{x_0}^{x} k_s(x')\,dx'\right]\right\} = \mathbf{A}\mathbf{E}\mathbf{b}_s \exp\left[\int_{x_0}^{x} k_s(x')\,dx'\right]. \tag{3}$$

Now introduce $\mathbf{\Omega} = \mathbf{E}^{-1}\, d\mathbf{E}/dx$. Upon carrying out the differentiation, cancelling the exponential term, and multiplying by $\mathbf{E}^{-1}$ there results, in component form,

$$\frac{db_{ss}}{dx} + \Omega_{ss} b_{ss} = -\sum_{j \neq s}^{N} \Omega_{sj} b_{js}, \tag{4}$$

$$(k_s - k_i)\, b_{is} + \Omega_{is} b_{ss} = -\frac{db_{is}}{dx} - \sum_{j \neq s} \Omega_{ij} b_{js},\ i \neq s, \tag{5}$$

$i, j = 1, \ldots, N$. The terms which are asymptotically dominant in the ratio of local wavelength to scalelength of $\mathbf{A}$ have been put on the left-hand side.

The advantages of this new scheme are: (i) the eigenfunctions $\mathbf{b}_s$ are smoothly varying functions similar to a normalized envelope of the oscillatory solution and consequently (mostly) independent of node number, and (ii) each stage of the scheme has known sources of error which can be controlled without increased computational overhead.

Define the rough smallness parameter ε_s,

$$\varepsilon_s(x) = \frac{\max |\Omega_{ij}|}{\min |k_s - k_i|} \ll 1 \qquad \text{for} \quad i \neq s. \tag{6}$$

Recall that in the limit, where $\mathbf{A}$ is constant, $d\mathbf{E}/dx = \mathbf{0}$ and, hence, $\mathbf{\Omega} = \mathbf{0}$ and Eq. (4) reduces to $db_{ss}/dx = 0$. Then (5) is consistent with $b_{is} = \delta_{is}$. When ε_s is small this suggests that we treat $b_{ss} \sim \mathcal{O}(1)$, $db_{is}/dx \sim \mathcal{O}(\varepsilon_s)$, $\Omega_{is} \sim \mathcal{O}(\varepsilon_s)$, and $b_{is} \sim \mathcal{O}(\varepsilon_s)$ for $i \neq s$. Correspondingly, to lowest order in ε_s, (4) can be approximated by

$$\frac{db_{ss}}{dx} \approx -\Omega_{ss} b_{ss}. \tag{7}$$

If we define $\kappa_{is}(x) = k_s - k_i$, then (5) can be approximated by

$$b_{is} \approx -\frac{\Omega_{is}}{\kappa_{is}} b_{ss}. \tag{8}$$

An approximation correct to next order in ε_s for b_{ss} may be obtained using (8) in (4) to give

$$\frac{db_{ss}}{dx} \approx \left[-\Omega_{ss} + \sum_{i \neq s} \frac{\Omega_{si}\Omega_{is}}{\kappa_{is}(x)} \right] b_{ss}. \tag{9}$$

Correspondingly, the approximation for b_{is} for $i \neq s$ can be improved by using (7) and (8) in (5) to obtain, for $i \neq s$,

$$b_{is} = \left[-\frac{\Omega_{is}}{\kappa_{is}} + \frac{1}{\kappa_{is}^2} \sum_{j \neq s} \Omega_{ij}\Omega_{js} + \frac{1}{\kappa_{is}} \frac{d}{dx}\left[\frac{\Omega_{is}}{\kappa_{is}}\right] - \frac{\Omega_{ss}}{\kappa_{is}} \frac{\Omega_{is}}{\kappa_{is}} \right] b_{ss}. \tag{10}$$

Note that on the right-hand side of (10) the first term in brackets is of order ε_s, while the other terms are of order ε_s^2. Equation (10) can be used in (4) to obtain an improved asymptotically approximate equation for b_{ss}, etc.

In practice when $N > 2$ and/or when $\mathbf{A}(x)$ is not known analytically, numerical solution of the problem is required. When the k_j are dominantly real and large it is best to employ (9) and (10) or their higher order counterparts to approximate the solution, since direct solution of (4) and (5) is an unstable process in virtue of the attendant stiffness of the system. The relative error can be gauged by examination of the ratio of the term of highest order in ε_s on the right-hand side of the counterpart of (10) to its immediate predecessor. The successive higher order derivatives which occur are required with successively lower accuracy, which relieves the burden of numerical differentiation.

When the k_j are large and predominantly imaginary, (4) and (5) can be successfully treated by direct integration. It is only neccessary to use initial conditions which are asymptotically correct. The point x_0 is chosen in the interval under consideration such that ε_s is a minimum and then we choose $b_{ss}(x_0) = 1$. The other $b_{js}(x_0)$ are determined recursively by solving

$$\sum_{j=1}^{N} \left[\Omega_{is}(x_0) + \kappa_{is}(x_0)\, \delta_{ij}\right] b_{js}^{(n+1)}(x_0) = -\frac{db_{is}^{(n)}(x_0)}{dx_0} \tag{11}$$

for $b_{js}^{(n+1)}(x_0)$ for $j \neq s$. The values for $b_{js}^{(1)}(x_0)$ may be obtained by approximating the right-hand side of (11) by zero. Using these initial data one then integrates (5) one small step in x from x_0 so as to determine the derivative term for use in (11), which then determines $b_{js}^{(2)}(x_0)$ etc. This process is continued until the desired asymptotic accuracy in $b_{ij}(x_0)$ is achieved for $s = 1, 2, \ldots, N$. Using these values as initial data (4) and (5) can be integrated stably using an implicit method which will serve to filter out any small amplitude rapidly varying corrections outside the desired accuracy.

When dealing with the unapproximated set (4) it is convenient in any domain where $\det |\mathbf{E}| \neq 0$ to normalize the eigenvectors to unity in a differentiable way, $\mathbf{e}_i^H \cdot \mathbf{e}_s = \delta_{is}$, where the superscript H denotes the Hermitian conjugate. Constructing the b_{ij} by this process yields a linearly independent, completely determined set $\mathbf{z}_s$, $s = 1, 2, 3, \ldots, N$, of solutions of the original equation (1). These form a basis

such that any solution can be written as a linear combination thereof, namely,

$$\mathbf{z} = \sum_{s=1}^{N} \alpha_s \mathbf{z}_s$$
$$= \mathbf{E} \sum_{s=1}^{N} \alpha_s \mathbf{b}_s \exp\left[\int_{x_a}^{x} k_s(x')\,dx'\right], \tag{12}$$

where the α_s are constants to be determined to satisfy initial and/or boundary conditions at a point x_a. Note that it follows from (1) and (12) that

$$\mathbf{E}(x_a)^{-1}\,\mathbf{z}(x_a) = \sum_{s=1}^{N} \alpha_s \mathbf{b}_s(x_a), \tag{13}$$

which is a system of N algebraic equations for the α_s. If we define the non-singular matrix $\mathbf{B} = [b_{is}]$ and the vector $\boldsymbol{\alpha} = [\alpha_s]$ then Eq. (13) can be written, suppressing the argument x_a, as $\mathbf{E}^{-1}\mathbf{z} = \mathbf{B}\boldsymbol{\alpha}$ and so $\boldsymbol{\alpha} = \mathbf{B}^{-1}\mathbf{E}^{-1}\mathbf{z}$.

2.2. *Numerical Treatment*

This particular scheme combines a variety of numerical techniques and ways of implementing them. An important consideration when testing this scheme will be its ability to maintain high accuracy with low computational overhead. In addition, major sources of error should be identifiable and correctable. A detailed description of each numerical component of our implementation of this method is beyond the scope of this paper and the reader is referred to Bernstein, Brookshaw, and Fox [11] for more details.

In general the parameters $\varepsilon_s(x)$ will not be uniformly small over the interval in x of interest. When $\varepsilon_s(x)$ is uniformly not small and there is no coalescence of roots k_j, the transformed equations may still be used, but often provide little advantage over the original system. More important is the situation where $\varepsilon_s(x)$ is small except in the neighborhood of a limited number of points where two or more of the k_j coalesce, or of singular points of (1). The most likely coalescence is binary, which is the only one we shall consider in detail here. In the examples in this paper this coalescence always takes place on the real axis. In the neighborhood of a binary coalescence the eigenvalues are either real or complex conjugate pairs. Instances of higher order coalescences are readily dealt with by an evident but tedious extension of the technique to be described.

Domains in x in which $\varepsilon_s(x)$ is suitably small we term *regular* (or **R**) regions. Domains in x where this is not so, commonly thin "boundary layers," we term *transition* (or **T**) regions. In **R**-regions it is efficient, accurate, and economical to solve the transformed equations as outlined above. In **T**-regions it is advantageous to solve the original system of Eq. (1). These solutions must be joined at the boundaries between the two types of regions, which is conveniently done using (12), (13), *et seq.*

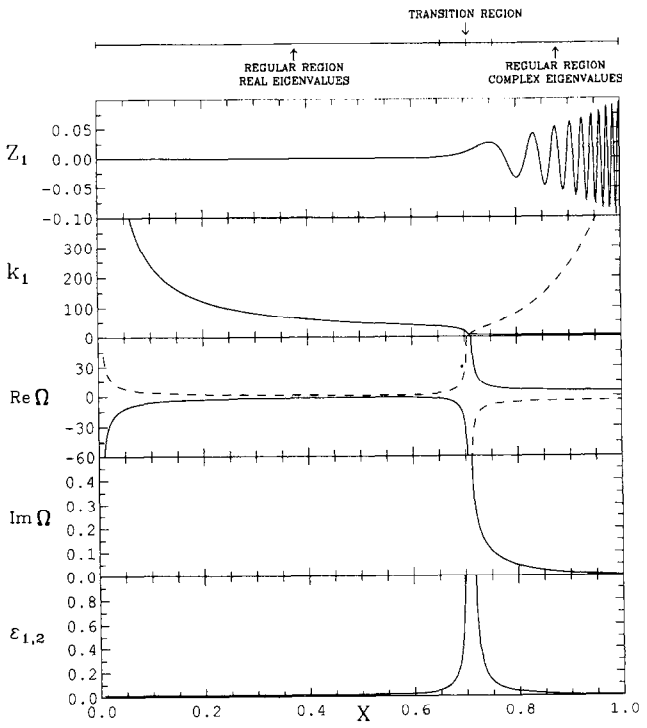

FIG. 1. Quantities related to the solution of the example in Section 3, with $\nu = 2$, $p = 10$, $q = 10$, and 20 nodes in the solution using the method of this paper: (a) a schematic of how the domain is divided into regular and transition regions; (b) the regular solution reconstructed from the transformed variables; (c) eigenvalue associated with the regular solution; in the first regular region there is only one component; in the second regular region the solid line is the real component and the dashed line is the positive imaginary component of the pair; (d) shows the real components of $\boldsymbol{\Omega}$, the solid line is Ω_{11} and the dashed line is Ω_{12}; (e) imaginary components of $\boldsymbol{\Omega}$, the solid line is Ω_{11} and the dashed line is Ω_{12} (overlayed); (f) the small parameter ε_s; note the rapid variation near the transition region.

In a given problem it is useful to first numerically generate the $k_j(x)$ over the domain and examine the results for exact or near coalescence. The $\varepsilon_s(x)$ could also be computed in order to establish if they are adequately small to warrant the use of the transformed equations. In practice, for computational speed, this is done after the domain has been subdivided. Figure 1a shows an example of how the domain was subdivided for the modified Bessel equation discussed in Section 3 below.

When there is a binary coalescence on the real axis, the theory of Appendix A applies and can be used to estimate the thickness of the **T**-region straddling the point of coalescence x_c. Namely, initially we choose the boundaries (x_c^- and x_c^+) of the **T**-region to be (see Appendix A)

$$x_c^- = x_c - \xi^- g'(x_c)^{-1/3}, \tag{14}$$
$$x_c^+ = x_c + \xi^+ g'(x_c)^{-1/3}, \tag{15}$$

where the discriminant $g(x)$ whose derivative appears in Eq. (14) and (15) is given by (A24). The point x_c can be accurately determined by finding the zero of the above discriminant expression which only involves the evaluation of simple properties of the coefficient matrix. The coefficients ξ^- and ξ^+ are typically of order 2.5 (see Appendix A) and are chosen on the basis of experiment to achieve the desired accuracy with minimum computational effort.

In the neighborhood of a singular point of (1) often the divergent solutions are characterized dominantly by $\exp \int k_j(x)$, in which event it is not necessary to develop a series solution about that point to start the solution; simply define $\mathbf{z}_s = \mathbf{E}\mathbf{b}_s \exp \int_{x_0}^{x} dx\, k_s(x)$ and start at any convenient point away from the singularity.

In the example ξ^+ corresponds to the side where the k_j are real. Then, ξ^+ and ξ^- are varied to as to achieve the desired accuracy. This can be done in such a way as to be common to all parameter variations of a given problem. Experience thus far has shown a remarkable insensitivity to the choice of ξ^-. However, one must choose ξ^+ so as to include at least one node of the oscillation; otherwise unacceptable errors may appear in the solutions.

The sensitivity of the results on the choice of the width of the T-region could be further reduced by incorporating an adaptive grid in the **R**-regions. The grid separation would decrease as the calculation approached the **T**-region. An adaptive grid could be constructed for specific cases to accommodate the change in the dependent variables as the solution approaches x_c and thus reduce the sensitivity (and accuracy dependence) of the results to the width of the T-region.

Another adjustable parameter in the scheme is the number of iterations to use in the initialization scheme for the eigenfunctions **B**. From inspection of the formal integration by parts the remainder for complex eigenvalues will oscillate about a mean. The use of an implicit integration scheme ensures stability and damps the oscillations that are a part of the solution due to the approximate initialization. Therefore, the number of terms used in the initialization of the transformed equations must be chosen so that the amplitude of the oscillating part of the solution does not contribute to the solution, to the required accuracy.

The approximation used to initialize the eigenfunctions **B**, is based on the small parameter ε_s. The naïve method would be to incorporate as many terms as required so that the last term is smaller than some specified accuracy requirement for the solution. This method ignores a number of points: first, each term in the series is calculated from a previous term using a numerical differentiation scheme which has a truncation error and, second, the final solution is a linear combination of functions and the effect of the error in the initialization is unknown. There is also a third point that should be noted: as the number of nodes in an **R**-region increases, the small parameter ε_s decreases; that is fewer terms are required in the initialization series for equivalent accuracy.

From the two examples presented in this paper the minimum number of terms required in the initialization series was two; that is, we require only terms to second order in the small parameter ε_s. This ensured five-figure accuracy in the solution for all examples described. The incorporation of more terms did not alter the solution, as the error was dominated by the truncation error in the differentiation and integration schemes.

3. EXAMPLE 1 (MODIFIED BESSEL EQUATION)

3.1. *Description*

A simple test of the method described above is provided by a linear second order ordinary differential equation whose coefficient matrix is

$$\mathbf{A}(x) = \begin{bmatrix} 0 & 1 \\ \dfrac{-(\lambda^2 q^2 x^{2q} + p^2 - v^2 q^2)}{x^2} & \dfrac{-(1-2p)}{x} \end{bmatrix}, \tag{16}$$

where v, λ, p, and q are positive constants and $0 \leqslant x \leqslant 1$. The variables are $\mathbf{z} = (z_1, z_2)$ with $z_2 = dz_1/dx$. The general solution of this equation is

$$z_1(x) = x^p(\alpha J_v(\lambda x^q) + \beta Y_v(\lambda x^q)), \tag{17}$$

where α and β are arbitrary constants. Near the origin,

$$z_1(x) \sim x^p \left[\frac{\alpha}{\Gamma(1+v)} \left(\frac{\lambda x^q}{2} \right)^v - \frac{\beta}{\Gamma(1-v)} \left(\frac{\lambda x^q}{2} \right)^{-v} \right] \tag{18}$$

and for regularity at the origin we must choose $\beta = 0$. The quantities J_v, Y_v, and Γ are Bessel functions of the first and second kind and the gamma function, respectively. For $\lambda x^q \gg v$ the asymptotic form of the solution is

$$z_1(x) \sim \alpha \sqrt{2/\pi}\, x^{p - q/2} \cos\left(\lambda x^q - \frac{v\pi}{2} - \frac{\pi}{4} \right). \tag{19}$$

The eigenvalues $k_{1,2}$ of the coefficient matrix are

$$k_{1,2} = -\frac{1-2p}{2x} \pm \frac{1}{2x} \sqrt{1 + 4v^2 q^2 - 4p - 4\lambda^2 q^2 x^{2q}}. \tag{20}$$

Note that there is one point where the eigenvalues coalesce, namely,

$$x_c = \left(\frac{1 + 4v^2q^2 - 4p}{4\lambda^2 q^2} \right)^{1/(2q)} \tag{21}$$

The eigenvectors $\mathbf{e}_1$ and $\mathbf{e}_2$ are arbitrary to within a multiplier which can be chosen for convenience.

Consider the case $p = 10$, $q = 10$, and $v = 2$ with 20 nodes in the solution (this latter will fix λ). Figure 1 displays a comparison of the solution z_1, the eigenvalue k_1, the real and imaginary parts of $\mathbf{\Omega}$ and the small parameters ε_1 and ε_2 over the domain. As expected, these figures indicate there is one coalescence point and, in the vicinity of this point, $\mathbf{\Omega}(x)$ is no longer slowly varying and ε_s becomes larger. In this example and the example of the next section the method of solution in the vicinity of $x = 0$ needs special consideration. Also note that near $x = 0$, $\mathbf{\Omega}$ starts to diverge as if there was an eigenvalue coalescence point at the origin. This is due to the singular nature of the coefficient matrix near the origin. The parameter ε_s in Fig. 1f, though, remains uniformly small near the origin implying that the transformed equations are valid in this region (cf. Section 4).

To find the regular solution of $\mathbf{z}$ in the numerical implementation, we need to exclude the irregular component (see (17)). This is easily achieved by using the solution constructed from the correct eigenvalue. From Section 2 we know that the final solution of an **R**-region is constructed from the linear combination of solutions generated from each eigenvalue. To ensure we follow the correct solution in the first **R**-region we follow only the solution constructed from the positive eigenvalue. That is the eigenvalue that produces a growing solution. This technique greatly simplifies the initialization of the method, though it does mean that if a unique solution $\mathbf{z}$ is required, it must be fixed by knowledge of the solution at a given point.

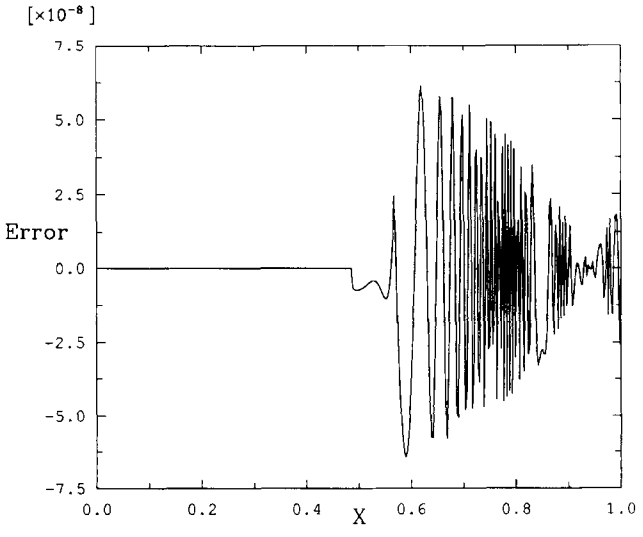

FIG. 2. The relative error in z_1, the solution of (1) using (16) with $v = 2$, $p = 10$, $q = 10$, $\xi^+ = 4$, $\xi^- = 1$, 320 nodes in the solution, 160 grid points in the **R**-region, and 80 grid points in the **T**-region.

3.2. *Results*

Equation (16) was chosen as a first test of the method because each step of the transformation could be calculated analytically. This was helpful in removing errors from each section of the numerical code. In describing the results we will restrict ourselves to comparing the final solution to the analytic solution primarily for simplicity. As an example of this, Fig. 2 shows the error in z_1, defined as the pointwise difference between the exact solution and the method solution divided by the envelope of the analytic solution. Note that since our method uses very few points in the oscillating region the error can be underestimated due to selection effects (see Table III).

The error in the final solution $\mathbf{z}$ is the accumulated error from a number of sources, although the dominant contribution to the error comes from the calculation of $d\mathbf{E}/dx$ and the integration of the **B** equations and, to a lesser extent, the characteristic exponent. Figure 1 clearly shows that if the **T**-region is too narrow the assumption that the transformed quantities vary slowly is no longer valid. The numerical truncation error in the vicinity of x_c will increase due to the growth of higher order derivatives. This could be alleviated by an adaptive grid, but a computationally simpler method is to use an appropriate **T**-region width.

The two parameters that fine tune the width of the **T**-region are ξ^- and ξ^+ of (14) and (15). Table I shows the effect on the error when ξ^+ is reduced. This parameter governs the transition halfwidth on the oscillating side of x_c for this example. Table II shows the effect on the error when ξ^- is reduced. This parameter governs the transition halfwidth on the exponential side of x_c. Both tables show that,

TABLE I

The Maximum Relative Error (as Defined in Section 3.2) for the Example in Section 3 as a Function of the Width of the **T**-region

		Maximum error	
ξ^+	Transition (right edge-x_c^+)	z_1	z_2
0.05	0.603	8.8×10^{-3}	8.3×10^{-3}
0.10	0.604	6.8×10^{-5}	6.6×10^{-5}
0.50	0.613	1.5×10^{-6}	1.4×10^{-6}
1.00	0.624	7.2×10^{-7}	6.5×10^{-7}

Note. $\xi^- = 4$, $p = 10$, $q = 10$, 100 nodes in the solution, 80 grid points in the **T**-region, and 160 grid points in the **R**-region. The coalescence point of the eigenvalues is $x_c = 0.602$. No nodes in the solution appear in the **T**-region over this range.

TABLE II

The Maximum Relative Error for the Example in Section 3 as a Function of the Width of the T-region

ξ^-	Transition (left edge-x_c^-)	Maximum error z_1	Maximum error z_2
1.0	0.876	8.9×10^{-4}	6.3×10^{-4}
2.0	0.868	1.6×10^{-4}	1.1×10^{-4}
3.0	0.860	4.1×10^{-5}	3.1×10^{-5}
4.0	0.852	1.3×10^{-5}	1.2×10^{-5}
5.0	0.844	2.6×10^{-6}	4.9×10^{-6}

Note. $\xi^+=2$, $p=10$, $q=10$, 10 nodes in the solution, 80 grid points in the T-region, and 160 grid points in the **R**-region. The coalescence point of the eigenvalues is $x_c=0.884$. No nodes in the solution appear in the T-region over this range.

as expected, to achieve five-digit accuracy the optimum values for both parameters is ~ 2.5. It should be stressed that for a particular problem both parameters need only be chosen once. The results of Appendix A furnish us a method for dynamically adjusting the width of the T-region as the index v and the number of nodes in the solution changes. In most problems this T-region is one which is not difficult to deal with using the original equations and so there is very little accuracy lost in converting between the transformed and original equations and back again.

The method is expected to easily deal with both oscillating and exponentially growing solutions with no change in the input parameters. Table III shows the effect on the error in z_1 as the number of nodes in the solution is increased, and Table IV shows the effect of increasing the index v on the solution. These results indicate that the error in the method is independent of the number of nodes in the solution. The decrease in the error as the number of nodes increases is due

TABLE III

The Maximum Relative Error for the Example in Section 3 as a Function of the Number of Nodes in the Solution

Nodes in solution	x_c	Maximum error z_1	Maximum error z_2
20	0.703	3.8×10^{-6}	3.7×10^{-6}
40	0.658	2.3×10^{-6}	1.1×10^{-6}
80	0.615	2.9×10^{-6}	2.9×10^{-6}
160	0.574	3.4×10^{-7}	3.1×10^{-7}
320	0.536	9.1×10^{-8}	9.1×10^{-8}
640	0.500	1.5×10^{-6}	1.5×10^{-6}

Note. $v=2$, $\xi^+=2$, $\xi^-=4$, $p=10$, $q=10$, 80 grid points in the T-region, and 160 grid points in the **R**-region.

TABLE IV

The maximum Relative Error for the Example in Section 3 as a Function of the Index v, with 10 Nodes in the Solution

Index v	x_c	Maximum error z_1	Maximum error z_2
2	0.750	1.4×10^{-6}	1.4×10^{-6}
4	0.798	5.8×10^{-7}	5.8×10^{-7}
8	0.843	6.4×10^{-5}	4.9×10^{-5}
16	0.884	1.3×10^{-5}	1.3×10^{-5}

Note. $\xi^+=2$, $\xi^-=4$, $p=10$, $q=10$, 80 grid points in the T-region, and 160 grid points in the **R**-region.

to a selection effect in the final solution, as we have less than one grid point per node (axis crossing). Equation (18) shows that increasing the index in this example differential equation increases the exponential behavior of the solution before it begins to oscillate. The error in the method shows no trends with changing index, though there is some variation.

To demonstrate that the majority of the error in the solution is due to truncation associated with the numerical differentiation and integration, Table V shows the effect of reducing the grid stepsize in the **R** and T-regions. The first entry in the table is probably too small due to selection effects as so few points are used. The almost identical error for the last two entries in the table is due to the initialization of the **B** equations. In this section the initialization is only to second order in the parameter ε_s, therefore the residual small amplitude oscillations in the transformed equations are not being resolved and this error now dominates. Apart from these accountable variations the trend in the table is as expected, the decrease in the steplength is reducing the truncation errors of the differentiation and integration schemes.

TABLE V

The Maximum Relative Error for the Example in Section 3 as a Function of the Number of Grid Points in Each Region

Number of grid points: Regular	Number of grid points: Transition	Maximum error z_1	Maximum error z_2
40	20	3.4×10^{-5}	3.2×10^{-5}
80	40	7.2×10^{-5}	7.1×10^{-5}
160	80	8.6×10^{-7}	8.4×10^{-7}
320	160	8.2×10^{-8}	8.0×10^{-8}
640	320	7.7×10^{-8}	7.8×10^{-8}

Note. $v=2$, $\xi^+=2$, $\xi^-=4$, $p=10$, $q=10$ and 50 nodes in the solution.

3.3. *Summary*

The test results in this section indicate that with a fixed number of grid points the scheme outlined in Section 2 can be used to calculate solutions of the example equation, independent of the number of oscillations (nodal points) or the exponential growth of the solution.

The results of this section also demonstrate that the accuracy of the solution does not critically depend on the choice of the two important parameters ξ^- and ξ^+ which govern the width of the T-region. There is a critical width, which depends on the desired accuracy, after which no change is made in the solution.

In this example we selected the regular solution by following the solution associated with the positive eigenvalue in the first regular region near the origin. For this case, where the parameters ε_s are uniformly small in the first regular region, this selection has been shown to be valid.

4. EXAMPLE 2 (NON-RADIAL OSCILLATIONS OF STARS)

4.1. *Introduction*

The equations governing non-radial oscillations of stars are those representing conservation of mass, momentum, and energy, together with an equation of state for the gas, an expression for the gravitational potential, equations for radiative transfer, and the magnetic field. For the purposes of this paper we shall assume the oscillations are adiabatic and neglect the effects of radiative transfer and magnetic fields.

The method of solution involves separating the equations into their mean parts (structure of the star) and fluctuating parts (the non-radial oscillation). The detailed derivation is beyond the scope of this paper and the reader is referred elsewhere [6, 12, 13]. The result of the separation is a fourth-order system of linear, ordinary differential equations. If we write

$$\mathbf{z} = [\xi, p', \Phi', d\Phi'/dr]^{\mathrm{T}}, \tag{22}$$

then (if r is the radial coordinate and R is the radius of the star), the coefficient matrix $\mathbf{A}(r)$, $0 \leqslant r \leqslant R$ of the equations is

$$\begin{bmatrix} -\frac{1}{\gamma p}\frac{dp}{dr} - \frac{2}{r} & -\frac{1}{\gamma p} + \frac{l(l+1)}{\omega^2 r^2 \rho} & \frac{l(l+1)G}{\omega^2 r^2} & 0 \\ \rho\omega^2 + \frac{dp}{dr}\left(\frac{1}{\gamma p}\frac{dp}{dr} - \frac{1}{\rho}\frac{d\rho}{dr}\right) & \frac{1}{\gamma p}\frac{dp}{dr} & 0 & -G\rho \\ 0 & 0 & 0 & 1 \\ 4\pi\rho\left(\frac{1}{\gamma p}\frac{dp}{dr} - \frac{1}{\rho}\frac{d\rho}{dr}\right) & \frac{4\pi\rho}{\gamma p} & \frac{l(l+1)}{r^2} & -\frac{2}{r} \end{bmatrix}. \tag{23}$$

The quantities ξ, p', and Φ', which depend on radius r, are the radial displacement, the perturbed pressure, and the perturbed gravitational potential, respectively; p is the unperturbed pressure, ρ is the unperturbed density, G is the gravitational constant, γ is the ratio of specific heats of the gas (for adiabatic oscillations $\gamma = \frac{5}{3}$ see [13]).

Part of the derivation of these equations involves an expansion in spherical harmonics which introduces the spherical harmonic indices l and m. For a spherically symmetric star with uniform rotation and no magnetic field there is complete degeneracy in the spherical harmonic index m and so modes are characterized by the spherical harmonic index l representing latitude variation and an index n ($-\infty < n < +\infty$) for the ordered eigenfrequencies, $\omega(l, n)$, to be determined and compared with observations of stars.

There are two classes of solutions admitted by the above set of equations, those corresponding to pressure driving (p-modes, whose eigenfrequencies go to ∞) and those due to buoyancy (g-modes, whose eigenfrequencies condense on zero). These two solutions are characterized by quite different ranges of the eigenfrequency ω. Further details on these classes of solution may be found in [12 or 13].

4.2. *Cowling Approximation*

In many stars, perturbations in the gravitational potential Φ' are small and are neglected (even though the error introduced is not always negligible) when calculating the non-radial oscillation modes. This approximation, first suggested by Cowling [14] reduces the fourth-order system to a second-order one. Both of these cases are suitable for demonstrating the properties of the method we have developed.

4.3. *Unperturbed State—Polytrope*

The expressions for the unperturbed quantities mentioned in the previous section may be reduced to a single second-order differential equation for the dimensionless density. If $y = (\rho(r)/\rho(0))^{1/s}$ and $x = r/R$ is the dimensionless distance, then

$$\frac{d}{dx}\left(x^2\frac{dy}{dx}\right) + x^2 y^s = 0. \tag{24}$$

The pressure is derived from the density using the so-called polytropic equation of state $p = p(0)\, y(x)^{1+1/s}$ (see [15]). In this example, the polytropic index s is 1.5.

A polynomial series solution was obtained for the above equation. In fact, two series were constructed around the points $x = 0$ and $x = 1$, with approximately 15 terms in each series [16]. Both series are slowly converging. Conversion between the two series was performed at the point where both series give acceptable accuracy.

The use of a series solution for the above equation was motivated by the desire to minimize the error from this part of the calculation so that any errors present reflect those of the method. The usual form of the unperturbed state in stellar oscillation calculations is a table of discrete values. The errors in such tables are those inherent to the generating program and the method of interpolation.

As stated above the unperturbed model is in dimensionless form and the results quoted below are also dimensionless. For the case of the sun the units for the eigenfrequency ω are $\sqrt{GM_\odot/R_\odot^3}/2\pi = 99.778\ \mu\text{Hz}$, where $M_\odot$ is the mass of the sun and $R_\odot$ is its radius.

4.4. *Parameters* (l, ω) *and the Boundary Conditions*

Two parameters appear in the equations for adiabatic nonradial oscillations of a star; the order of the spherical harmonic l and the eigenfrequency ω. For the purposes of this paper we will only concern ourselves with one class of solutions, the p-modes, since a value of $s = 1.5$ excludes g-modes from the solution, see [13].

To investigate how the choice of l will affect our solution we can expand ξ and p' in powers of a small stepsize δx around the origin. To first order the regular solution behaves as

$$\xi \propto \delta x^{l-1}, \tag{25}$$

$$\frac{p'}{\rho} \propto \frac{\delta x^l \omega^2}{l}. \tag{26}$$

The above equations and the results of Section 3 show that near the origin the solution for the non-radial oscillation equations behave similiarly to the regular solutions of the modified Bessel equation. This implies that, as with the index v for the Bessel function, as l is increased the coalescence point will move toward the outside boundary. Thus for a given number of nodes, as l is increased the average wavelength of the solution will decrease.

The parameter ω is ultimately constrained by the choice of the unperturbed state and the surface boundary condition (for a fuller discussion of the surface boundary condition see [12]). The eigenfrequency ω will be real, for example, if the perturbed pressure is zero at the surface. This means that for a fixed l there will be a family of discrete solutions with an increasing number of nodes (n), each with a discrete eigenfrequency ω. As with the Bessel equation example, and as can be seen from Eq. (26), the eigenvalue coalescence point (the singularity in the transformed equations) will move closer to the origin as the number of nodes in the solution increases.

4.5. *Methods of Solution for Comparison*

The equations for non-radial oscillations of a star with center and surface boundary conditions constitute a standard boundary value problem, with a number of standard methods for their solution. Traditionally, two techniques have been used, relaxation methods to solve the coupled algebraic equations formed by differencing the equations [13], or a shooting method using a high order integration method such as fourth-order Runge–Kutta scheme [17].

Both methods require the solution around the origin to be pre-computed via a Taylor series expansion. More importantly the discretization of the computational domain is dictated by the local wavelength of the solution.

We will be comparing the method outlined in Section 2 with a direct technique. The direct technique we use is an adaptive fourth-order Runge–Kutta method [18]. Unfortunately the direct method was not accurate enough to solve the equations in their standard form. The reason is that the near singular behaviour at the outer boundary causes the amplitude of the solution ξ to grow, usually by many orders of magnitude, though it is finite at the boundary. The

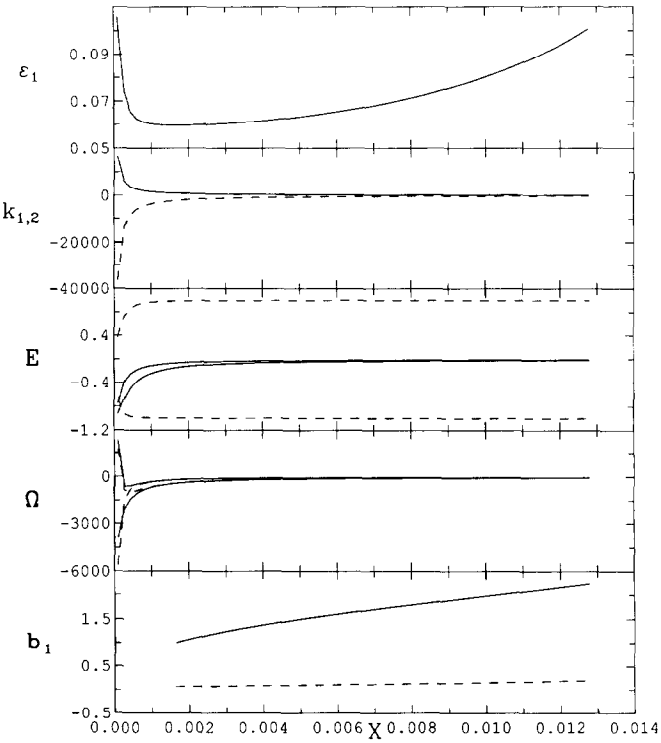

FIG. 3. Quantities related to the calculation of normal modes of non-radial oscillations in a star as described in Section 4, using the method of this paper. The Cowling approximation was used ($N = 2$) with $l = 2$ and 68 nodes in the solution. This figure represents the first **R**-region of the calculation where the eigenvalues are real: (a) the small parameter ε_1; note its magnitude and where the minimum occurs; (b) the eigenvalue components (note the divergence near the origin and that the regular solution is chosen from the positive component); (c) components of the eigenvector matrix; (d) the components of $\mathbf{\Omega}$; and (e) the eigenfunctions **B** of the regular solution; the diagonal component (solid line) is initialized to unity at the point where ε_1 is a minimum and the off-diagonal element (dashed line) is small (it is initialized as discussed in Section 2).

adaptive algorithm was incapable of producing accurate results in this region. To resolve this, the variables $U = \xi\rho r^2$ and $V = p'/\rho$ were adopted. At the outer boundary the amplitude of the variable U is bounded and therefore accurate solutions are obtainable with the adaptive algorithm.

An important simplification obtained by using the transformed system of equations outlined in Section 2 is the ability to identify the regular solution without having to develop a series, or other, solution in the neighborhood of the origin. The solution for the transformed system is constructed from a linear combination of amplitudes and the characteristic exponent based on the eigenvalues and near the origin, one solution will be unbounded. In this same region there will be two eigenvalues, one eigenvalue will be positive and one will be negative. The positive eigenvalue is associated with the regular growing solution and the negative eigenvalue is associated with the decaying irregular solution. By discarding the solution constructed with the negative eigenvalue we are sure to follow the regular solution.

Note that in Fig. 3a it appears that the parameter ε_1 is unbounded near the origin. This would suggest that the method for defining the regular solution will produce errors for this problem (cf. Section 3.1). By expanding the coefficient matrix **A** in powers of r and retaining the dominant terms we can calculate the eigenvalues, $\boldsymbol{\Omega}$ and **B** near the origin. From this we find that ε_1 remains bounded and is less than one near the origin, and therefore the positive eigenvalue will produce the regular solution.

In this particular example of our method the diverging behaviour of the equations near the outer boundary is in fact similar to a **T**-region in the interior. Note the imaginary components of the eigenvectors shown in Figs. 4d, e which tend to zero at the outer boundary. As with a coalescence point, the effect is to produce a near singular point in the transformed equations, see Fig. 5 for $\boldsymbol{\Omega}$ and the eigenfunctions $\mathbf{b}_s$. So, near $x = 1$ we transform to the U, V variables and solve the equations directly. By performing a boundary

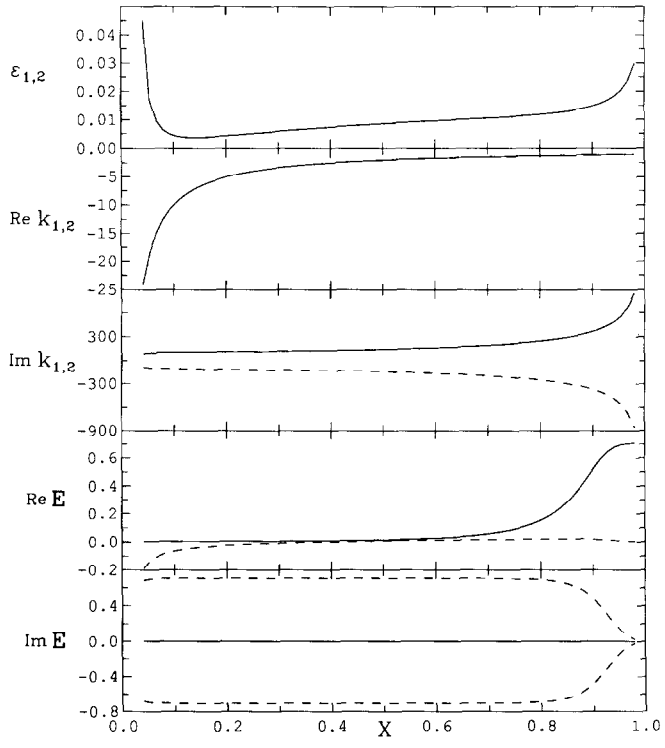

FIG. 4. Quantities related to the calculation of normal modes of nonradial oscillations in a star as described in Section 4, using the method of this paper. This figure covers the second **R**-region, where the eigenvalues are complex conjugate pairs of the case described in Fig. 3. (a) the small parameters ε_1 and ε_2 which are virtually identical, note the magnitude and where the minimum occurs; (b) the real components of the eigenvalues; (c) the imaginary components of the eigenvalues; (d) the real components of the eigenvector matrix; (e) the real components of the eigenvector matrix.

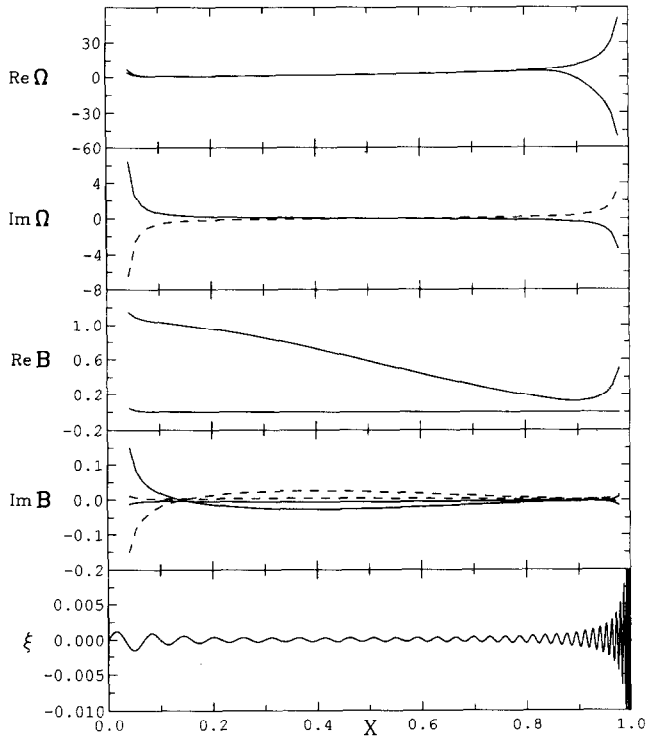

FIG. 5. Quantities related to the calculation of normal modes of nonradial oscillations in a star as described in Section 4, using the method of this paper. This figure is a continuation from Fig. 4. (a) the real components of $\boldsymbol{\Omega}$ (note the rapid variation near the outer boundary); (b) the imaginary components of $\boldsymbol{\Omega}$ (note the rapid variation near the transition region to the left and the outer boundary to the right); (c) the real components of the eigenfunctions **B** (note the smooth variation compared to the rapid variation in (e)); (d) the imaginary components of the eigenfunctions **B** (note the small variations around the axis and divergence near the transition region); (e) ξ, the first component of the original variables (radial displacement) reconstructed from the transformed variables (see Section 2) and scaled with unit maximum amplitude at $x = 1$.

layer analysis appropriate to the equations for the U, V variables near $x = 1$ we construct a method for specifying the width of the outer boundary layer by choosing how many nodes we require. To ensure accuracy we use a fixed grid fourth-order Runge–Kutta integration scheme. The preceding boundary layer analysis gives the approximate position of each node in the outer boundary layer and this information is used to integrate the equations using a fixed number of points per node.

In this example we will compare the accuracy of the method outlined in Section 2 by comparing the eigenfrequency ω with that obtained from the direct method. As a further comparison, we compare with some results for limited l and ω by Mullan and Ulrich [19] (MU) that are accurate to six significant figures.

4.6. *Results for the Cowling Approximation*

As in the previous example there is only one coalescence point in the domain whose position is a function of l and ω. Figure 3 shows the transformed variables in the **R**-region where all the eigenvalues are real. Near the origin, because of the singular nature of the coefficient matrix, the eigenvalues and $\mathbf{\Omega}$ are diverging. The eigenfunctions **B** show that they were initialized at the minimum of the parameters ε_s, $s = 1, 2$. Figures 4 and 5 show the transformed variables in the **R**-region, where the eigenvalues are complex conjugate pairs. Both figures show the full domain. The gap near the origin contains the first **R**-region and the **T**-region and the gap near the surface contains the outside boundary layer. From these figures it is easy to see that $\mathbf{\Omega}$ and the eigenfunctions **B** are very smooth and slowly varying over most of the **R**-region but they begin to diverge in the vicinity of the **T**-regions and at the outside boundary. This slow variation is the key to the fast and accurate solution of the equations in these regions.

In finding the solution, both the direct method and the transformed method use the same calculation of the unperturbed model and the same method and tolerance for convergence of the eigenfrequency. The eigenfrequency was considered converged if the absolute value of the correction was less than 5×10^{-6} relative to the eigenfrequency. MU used a different criterion for constructing their models and eigenfrequencies and consequently it is unlikely that a comparison between them will produce agreement to the very high accuracy we are interested in.

A comparison between the three methods is presented in Table VI. The eigenfrequency is listed for each method as

TABLE VI

A Comparision of the Elapsed CPU Times (64-bit Word) for One Integration Sweep from the Center to the Edge to Calculate One Normal Mode Non-radial Oscillation of a Star, Using the Transformed Equations (the New Scheme) and a Direct Integrator (See Section 4.5 for Details)

		Transformed		Direct		
l	Nodes	ω_T	Time	ω_D	Time	ω_{MU}
2	12	19.9154	17.9	19.9143	13.7	19.9149
2	19	30.0283	17.5	30.0273	18.2	30.0282
2	32	48.7435	17.7	48.7417	26.2	48.7431
3	10	17.5997	17.6	17.5983	13.8	17.5988
3	19	30.6661	17.6	30.6649	19.3	30.6658
3	32	49.4102	17.9	49.4085	27.4	49.4099

Note. In addition the calculated eigenfrequencies, in non-dimensional units, are also listed for the two methods and from the results of MU [19]. These calculations were performed using the Cowling approximation ($N = 2$), with 1 to 2 nodes of the solution in the **T**-region, 75 grid points in the **T**-region, 75 grid points in the **R**-region, and approximately 75 points per node in the boundary layer.

TABLE VII

A Comparision of the Elapsed CPU Timees (64-bit Word) for One Integration Sweep of Each Method as Described in Table VI as a Function of Increasing Wavenumber l and Nodes in the Solution

			Transformed		Direct	
l	Nodes	N_{Bl}	ω_T	Time	ω_D	Time
2	68	9	100.472	20.3	100.473	48.9
2	124	16	180.900	22.6	180.899	84.4
2	206	30	300.086	28.6	300.085	138
3	66	10	99.7301	20.5	99.7290	49.1
3	117	16	170.116	22.6	170.113	80.3
3	151	25	220.381	26.6	200.378	103
3	207	30	300.793	28.8	300.795	140
5	66	10	101.090	20.4	101.089	49.7
5	108	16	160.012	22.6	160.011	75.4
5	150	20	220.345	24.5	220.342	102
5	206	30	300.773	28.7	300.768	140
50	51	10	101.096	20.8	—	—
50	97	16	170.510	22.8	—	—
50	152	21	251.317	24.7	—	—
50	200	26	321.130	26.8	—	—
100	155	21	281.494	25.2	—	—
100	201	26	350.036	26.8	—	—
200	125	15	275.092	21.0	—	—
200	187	31	375.424	26.7	—	—
200	237	31	451.090	29.4	—	—

Note. These calculations were performed using the Cowling approximation ($N = 2$), with 75 grid points in the **T**-region, 75 grid points in the **R**-region, and approximately 75 points per node in the solution in the outer boundary layer (which is also listed).

units

well as the processing time (all times quoted are for a VAX station II running VAX/VMS with a Fortran 64-bit word) taken to calculate the solution from the converged eigenfrequency. We can see that both the direct and the transformed methods produced accurate results but the time taken for the transformed method is substantially constant while the time for the direct solution increases with the number of nodes. The maximum number of nodes in the solution in this table reflect the results published by MU [19].

Table VII extends the nodal and spherical harmonic index range of Table VI. As in Table VI, the eigenfrequency and the time taken are tabulated for our method and the direct method. Also tabulated is the number of nodes that need to be incorporated in the outer boundary layer used in the transformed method, to ensure accuracy. The number of nodes in the outer boundary layer is approximately 15% of the total number of nodes in the solution and accounts for the increase in time that occurs with increased nodes. This feature is peculiar to this example and is not a feature of the general numerical method.

The blanks in the table for large values of l reflect the lack of solutions from the direct method. To obtain solutions for large l the equations have to be transformed, removing the r^{l-1} dependence from the solutions, with the initial conditions modified accordingly. For these tests this was not considered necessary.

The preceding tables display the most accurate solution obtained from the transformation method. To obtain each entry in the table some of the parameters in the method were varied to test the sensitivity of the solution. Table VIII shows the sensitivity of the results to the input parameters.

TABLE VIII

A Comparison of the Sensitivity of the Computed Eigenfrequencies (in Non-dimensional Units) to the Number of Points per Region (Transition and Regular), Width of the T-region (Reflected by ξ^+ and ξ^-), and the Number of Nodes in the Boundary Layer N_{BI}

Points	ξ^+	ξ^-	N_T	N_{BI}	Time	ω
75	0.5	2.0	0	21	24.7	281.477
	2.0		1		25.1	281.494
	4.0		1		25.2	281.494
	6.0		2		24.7	281.495
75	4.0	6.0	1	21	24.8	281.494
		0.5	1		24.9	281.491
75	4.0	2.0	1	16	22.9	281.603
				31	29.0	281.491
150	4.0	2.0	1	21	49.2	281.493

Note. N_T is the resulting number of nodes in the solution in the T-region. The total number of nodes in the solution was 155 with $l = 100$.

In this example each region was subdivided into an equal number of grid points, that is, the **T**-region and the **R**-region and the number of points per node in the outer boundary layer.

This table demonstrates the insensitivity of the solution to the parameter ξ^- which specifies the transition width on the side with real eigenvalues and that one node in the transition on the side with imaginary eigenvalues ensures accurate solutions. All of the results in the tables have been run for 75 and 150 grid points in each region and no significant differences have been found.

What is obvious is that the number of nodes in the outer boundary layer is important; with too few, errors begin to appear in the solution; with too many, the time to integrate through the domain increases. It should be remembered that the importance of the outer boundary layer is a reflection of the problem being discussed, not the method. As stated above, standard techniques suffer because of the growing amplitude of the solution and the singular behavior of the coefficient matrix in this region.

4.7. *Full Fourth-Order System*

Thus far, the examples we have discussed have only been for second-order systems. Using a regularity condition at the origin and the boundary condition that the perturbed potential must match to the unperturbed vacuum solution in the exterior region, the fourth-order system may be solved.

As in the case of the Cowling approximation our method uses the behaviour of the eigenvalues near the origin to find the regular solution. For this problem there will be two eigenvalues corresponding to two growing regular solutions and these will be followed to the outer boundary and linearly combined to satisfy the two boundary conditions.

Table IX gives the results for a limited number of nodes and compares the times and eigenfrequencies against the direct method. The results of the two methods are in good

TABLE IX

A Comparison of the Elapsed CPU Times (64-bit Word) and Computed Eigenfrequencies for One Integration Sweep of Each Method as Described in Table VI

		Transformed		Direct	
l	Nodes	ω_T	Time	ω_D	Time
2	20	31.3964	61.8	31.3953	36.0
2	68	100.451	66.5	100.450	78.6
2	109	160.780	76.6	160.780	112
2	208	300.511	87.1	—	—

Note. These calculations were performed using the unapproximated equations ($N = 4$), with 75 grid points in the **T**-region, 75 grid points in the **R**-region, and approximately 75 points per node in the boundary layer.

agreement. The time taken has increased relative to the Cowling approximation results; this is not surprising since in both cases two solutions have to be integrated to match the two boundary conditions at the outside edge. The direct method has approximately doubled in computational time and the transformed method has nearly tripled. Again this is not surprising as the transformed method is now solving for quantities in a 4 by 4 coefficient matrix where before it was a 2 by 2.

4.8. *Discussion*

In this example the equations for non-radial stellar [illegible] for l and n. Difficulties encountered with the outside boundary layer are not a product of the method employed, but the problem. MU state that to achieve 6-figure accuracy in the eigenfrequency they require for their adaptive Runge–Kutta method $\sim 24\%$ of the points in the outer loop of the function ξ and ~ 70 points per node in the remainder of the domain. This is for a solution with 37 nodes. Using the method of this paper we require, to achieve better than 5-figure accuracy, ~ 75 points in the **R**-region that covers 85% of the nodes and only ~ 75 points per node in the outer 15% using the transformation to the U, V variables.

It is clear from the results and from tests not presented here that considerable computational time is taken up with the calculation of eigenvectors, eigenvector derivatives, and $\mathbf{\Omega}$, and with most of the computational time involved with the integration of **B**, but this time is offset by the relatively few points that need to be used in the computational domain. More important is that the time taken is independent of the number of nodes in the solution, which is clearly illustrated by the examples presented here.

5. SUMMARY

In this paper a numerical method has been presented which allows the accurate and efficient solution of systems of linear ordinary differential equations when the solutions vary rapidly relative to the coefficients of the variables. For a typical solution which oscillates with many nodes and with rapidly varying wavelength and amplitude, this method has many advantages over the usual solution by direct techniques or approximation by analytic techniques. In addition to computational efficiency this technique presents the results in a compact way. In many circumstances it precludes the need for series solutions near singular points. It also lends itself to efficient use of the results for computing integrals. Most importantly, this method has known sources of error which can be controlled without a substantial increase in computation times.

In the numerical part of this paper we have attempted to demonstrate the general applicability of this method and used the examples as a guide for implementation. Our approach for these examples was to favor simplicity over sophistication so as to make clear the methodology. For this reason the timing and accuracy results presented here should not be viewed as the best achievable for this method. Many improvements are possible, at the price of intricate programming. Some of these are under investigation and will be presented in subsequent papers.

This work was supported by grants from ONR under Contract N00014-B3-K-0610 (IBB and LB) and NASA under Grant NAGW-777 (PAF). The authors acknowledge discussions with P. Demarque, D. Guenther, S. Kawaler, and S. Sofia. The figures in this paper were produced [illegible] appreciated.

A. APPENDIX

A1. *Reduction in Order for an Nth-Order System*

We wish to derive an approximate solution valid in the neighborhood of a point where two eigenvalues coalesce. This can be used to estimate the halfwidth δ of the boundary layer straddling a point of coalescence x_c within which one must revert to the original equation for numerical integration. The width can be expressed in invariant fashion in terms of the other eigenvalues and the trace and determinant of **A**. The calculation reduces the problem to consideration of the Airy equation, just as for a turning point analysis in the WKB theory for a linear second order ordinary differential equation.

Consider the eigenvalue equation $\mathbf{A}(x)\,\mathbf{e}_j(x) = k_j(x)\,\mathbf{e}_j(x)$, where $\mathbf{A} = [A_{ij}]$ is an $N \times N$ matrix, $\mathbf{e}_j = [e_{ij}]$ an N-dimensional column vector, and x is a parameter. One can write alternatively in component form $A_{is}e_{sj} = k_j e_{ij}$, where the column index j is that of $\mathbf{e}_j$. Suppose that at x_c the eigenvalues are indexed so that $k_1(x_c) = k_2(x_c) = k_c$, and that in the neighborhood of x_c the eigenvalue k_c is well separated from the other eigenvalues $k_3(x)$, $k_4(x)$, ..., $k_N(x)$ which are distinct. Then in general there is but a single limiting eigenvector

$$\mathbf{e}_2(x_c) = \lim_{\varepsilon \to 0} \mathbf{e}_2(x_c + \varepsilon) = \lim_{\varepsilon \to 0} \mathbf{e}_1(x_c + \varepsilon) \qquad \text{(A1)}$$

associated with k_c, and the set of eigenvectors $\mathbf{e}_j(x_c)$, $j = 2, 3, 4, ..., N$, are linearly independent. Choose $\mathbf{n}_j = \mathbf{e}_j$, $j = 2, 3, ..., N$, and pick slowly varying vectors $\mathbf{n}_1$ and $\mathbf{n}_2$ so that the set $\mathbf{n}_j$, $j = 1, 2, 3, ..., N$, are linearly independent. Define $\mathbf{V} = [\mathbf{n}_1, \mathbf{n}_2, ..., \mathbf{n}_N] = [n_{ij}]$, then $\det \mathbf{V} \neq 0$, $\mathbf{V}^{-1}$ exists and

$$\mathbf{V}^{-1}\mathbf{A}\mathbf{V} = [\mathbf{V}^{-1}\mathbf{A}\mathbf{n}_1, \mathbf{V}^{-1}\mathbf{A}\mathbf{n}_2, k_3\delta_{i3}, ..., k_N\delta_{iN}]. \qquad \text{(A2)}$$

Assume that none of the set $k_3, k_4, ..., k_N$ vanishes in the domain under consideration. Then, by suitable column operations, we can put $\mathbf{V}^{-1}\mathbf{AV}$ in echelon form [10]. Namely, there exists a matrix $\mathbf{U}(x)$ such that

$$\mathbf{U}^{-1}\mathbf{AU} = \begin{bmatrix} C_{11}(x) & C_{12}(x) & 0 & 0 & \cdots & 0 \\ C_{21}(x) & C_{22}(x) & 0 & 0 & \cdots & 0 \\ 0 & 0 & k_3(x) & 0 & \cdots & 0 \\ 0 & 0 & 0 & k_4(x) & \cdots & 0 \\ \vdots & \vdots & \vdots & \vdots & \ddots & \vdots \\ 0 & 0 & 0 & 0 & \cdots & k_N(x) \end{bmatrix} \tag{A3}$$

and the components $C_{ij}(x)$ of the 2×2 matrix $\mathbf{C}$ are analytic in the neighborhood of the point x_c.

Let ζ be a column vector with N components $\zeta_i(x)$. Write

$$\mathbf{z} = \mathbf{U}\zeta \exp[k_c(x - x_c)] \tag{A4}$$

and insert the expression in $d\mathbf{z}/dx = \mathbf{Az}$. On distributing the derivative and multiplying on the left by $\mathbf{U}^{-1}\exp[-k_c(x-x_c)]$ there results

$$\frac{d\zeta}{dx} + \mathbf{\Gamma}\zeta + k_c\zeta = \mathbf{U}^{-1}\mathbf{AU}\zeta, \tag{A5}$$

where

$$\mathbf{\Gamma} = \mathbf{U}^{-1}\frac{d\mathbf{U}}{dx}. \tag{A6}$$

In component form (A5) yields

$$\frac{d\zeta_1}{dx} + k_c\zeta_1 + \sum_{j=1}^{N} \Gamma_{1j}\zeta_j = C_{11}\zeta_1 + C_{12}\zeta_2, \tag{A7}$$

$$\frac{d\zeta_2}{dx} + k_c\zeta_2 + \sum_{j=1}^{N} \Gamma_{2j}\zeta_j = C_{21}\zeta_1 + C_{22}\zeta_2, \tag{A8}$$

and for $j = 3, 4, ..., N$,

$$(k_j - k_c)\zeta_j - \Gamma_{j1}\zeta_1 - \Gamma_{j2}\zeta_2 = \frac{d\zeta_j}{dx} + \sum_{i=3}^{N} \Gamma_{ji}\zeta_i. \tag{A9}$$

Suppose that in neighborhoods adjacent to but outside a boundary layer of thickness 2δ centered on the point x_c that the small parameter $\varepsilon \ll 1$. Then at $x_c - \delta$ the theory of Section 2 applies. Suppose that $\mathbf{z}(x_c - \delta)$ corresponds to the solution with eigenvalue $k_1(x_c - \delta)$. Then, for one linearly independent solution, $b_1(x_c - \delta)$ is of order unity and all the other $b_j(x_c - \delta)$ are of order ε. Since $\mathbf{n}_j(x_c - \delta) = \mathbf{e}_j(x_c - \delta)$ for $j = 3, 4, ..., N$, we can choose the corresponding $\zeta_j(x_c - \delta) = b_j(x_c - \delta)$ which are of order ε, and these should remain small in the thin boundary layer. The components $\zeta_1(x_c - \delta)$ and $\zeta_2(x_c - \delta)$ are linear combinations of all the $b_j(x_c - \delta)$ via the inverse of (A4), namely they are given by the one and two components of $\zeta = \mathbf{U}^{-1}\mathbf{z}\exp[-k_c(x - x_c)]$, evaluated at $x = x_c - \delta$. They are in general both of order unity and should remain so within the boundary layer. Moreover, within the boundary layer we expect that $\min |k_j - k_c| \gg \max |\Gamma_{ij}|$. Then for $j = 3, 4, ..., N$, to lowest order in the small parameter ε which underlies the quasi-WKB limit, neglecting the terms on the right-hand side of (A9) yields

$$\zeta_j \approx \frac{\Gamma_{j1}\zeta_1 + \Gamma_{j2}\zeta_2}{k_j - k_c}, \qquad j = 3, 4, ..., N, \tag{A10}$$

and the terms in the sums in (A7) and (A8) are second order in the small parameter prevailing in the boundary layer compared with the derivative terms. Moreover, in the boundary layer one can make a Taylor series expansion of the C_{ij} to obtain to lowest significant order equations for ζ_1 and ζ_2,

$$\frac{d\zeta_1}{dx} + k_c\zeta_1 = C_{11}\zeta_1 + C_{12}\zeta_2, \tag{A11}$$

$$\frac{d\zeta_2}{dx} + k_c\zeta_2 = C_{21}\zeta_1 + C_{22}\zeta_2. \tag{A12}$$

It is convenient to introduce the new dependent variables

$$\eta_1 = \zeta_1 \exp\left[\int_{x_c}^{x} dx\,(k_c - C_{11})\right] \tag{A13}$$

$$\eta_2 = \zeta_2 \exp\left[\int_{x_c}^{x} dx\,(k_c - C_{22})\right]. \tag{A14}$$

Then (A11) and (A12) imply

$$\frac{d\eta_1}{dx} = C_{12}\eta_2 \exp\left[\int_{x_c}^{x} dx\,(C_{22} - C_{11})\right], \tag{A15}$$

$$\frac{d\eta_2}{dx} = C_{21}\eta_1 \exp\left[\int_{x_c}^{x} dx\,(C_{11} - C_{22})\right]. \tag{A16}$$

At x_c the eigenvalues of the 2×2 matrix $[C_{ij}]$ must be both k_c, since $\mathbf{A}$ and $\mathbf{U}^{-1}\mathbf{AU}$ have the same eigenvalues. Thus

$$\begin{vmatrix} C_{11}(x) - k_c & C_{12}(x) \\ C_{21}(x) & C_{22}(x) - k_c \end{vmatrix} = 0 \tag{A17}$$

and so

$$k_c = \frac{C_{11}(x_c)+C_{22}(x_c)}{2} \pm \sqrt{\left(\frac{C_{11}(x_c)-C_{22}(x_c)}{2}\right)^2 + C_{12}(x_c)\,C_{21}(x_c)}. \quad \text{(A18)}$$

Clearly in order that k_c be a double root, $C_{11}(x_c)=C_{22}(x_c)=k_c$ and $C_{12}(x_c)\,C_{21}(x_c)=0$. But the elements $C_{ij}(x)$ are presumably slowly varying throughout the boundary layer; thus we can approximate $C_{12}(x)$ and $C_{21}(x)$ by the linear term in the Taylor series in x. Moreover,

$$\begin{aligned}\exp\left[\int_{x_c}^{x} dx\,(C_{11}-C_{22})\right] &= \exp\left[\int_{x_c}^{x} dx\left(\frac{dC_{11}(x_c)}{dx}-\frac{dC_{22}(x_c)}{dx}\right)(x-x_c)+\cdots\right] \\ &= 1+\mathcal{O}[(x-x_c)^2]. \end{aligned} \quad \text{(A19)}$$

In the boundary layer, if we assume that $C_{21}(x_c)$ vanishes but that $C_{12}(x_c)$ does not, (A15) and (A16) reduce to

$$\frac{d\eta_2}{dx} = (x-x_c)\frac{dC_{21}(x_c)}{dx_c}\eta_1, \quad \text{(A20)}$$

$$\frac{d\eta_1}{dx} = C_{12}(x_c)\,\eta_2. \quad \text{(A21)}$$

If η_2 is eliminated there results

$$\frac{d^2\eta_1}{dx^2} = (x-x_c)\,C_{12}(x_c)\frac{dC_{21}(x_c)}{dx_c}\eta_1. \quad \text{(A22)}$$

Define

$$\begin{aligned} g(x) &= \left(\frac{C_{11}(x)-C_{22}(x)}{2}\right)^2 + C_{12}(x)\,C_{21}(x) \\ &= \left(\frac{C_{11}(x)+C_{22}(x)}{2}\right)^2 \\ &\quad + C_{12}(x)\,C_{21}(x) - C_{11}(x)\,C_{22}(x) \\ &= \frac{1}{4}(\text{Trace }\mathbf{C})^2 - \det \mathbf{C} \quad \text{(A23)} \\ &= \frac{1}{4}\left(\text{Trace }\mathbf{A}(x) - \sum_{j=3}^{N} k_j(x)\right)^2 \\ &\quad - \frac{\det \mathbf{A}(x)}{\prod_{j=3}^{N} k_j(x)} \quad \text{(A24)} \end{aligned}$$

which is the discriminant that must vanish at $x=x_c$ in order for a coalescence of an eigenvalue pair. Note that, since $C_{11}(x_c)=C_{22}(x_c)$ and $C_{21}(x_c)=0$, it follows that

$$\frac{dg\,(x_c)}{dx_c} = C_{12}(x_c)\frac{dC_{21}(x_c)}{dx} \quad \text{(A25)}$$

and (A22) becomes

$$\frac{d^2\eta_1}{dx^2} = (x-x_c)\frac{dg(x_c)}{dx_c}\eta_1. \quad \text{(A26)}$$

The general solution of (A26) is a linear combination of the Airy functions, namely $Ai[(x-x_c)(dg(x_c)/dx_c)^{1/3}]$ and $Bi[(x-x_c)(dg(x_c)/dx_c)^{1/3}]$, where the dominant asymptotic behaviors are given for $y \gg 1$ by

$$\begin{aligned} Ai(y) &\sim \frac{\exp((-2/3)\,y^{3/2})}{\pi^{1/2}y^{1/4}}; \\ Bi(y) &\sim \frac{\exp((2/3)\,y^{3/2})}{\pi^{1/2}y^{1/4}}, \\ Ai(-y) &\sim \frac{\sin((2/3)\,y^{3/2}+\pi/4)}{\pi^{1/2}y^{1/4}}; \\ Bi(-y) &\sim \frac{\cos((2/3)\,y^{3/2}+\pi/4)}{\pi^{1/2}y^{1/4}}. \end{aligned} \quad \text{(A27)}$$

It can be readily shown using these asymptotic forms and the limiting behavior of the WKB results, $z_1(x) \sim b_1(x)\exp\int_x^{x_c} dx/k_1(x)$, $z_2(x)\sim 0$, that the linear combination of Airy functions can be chosen so as to effect an asymptotic matching of the solutions. We will not carry this out here, since we are concerned only with defining the width δ of the boundary layer for use in branching in the numerical solution. It is adequate to note that this corresponds roughly to the change in y required for the solution to become asymptotic, which is roughly $y \sim 2.5$. This implies that the halfwidth of the boundary layer is

$$\delta \sim 2.5\frac{dg(x_c)^{-1/3}}{dx_c}. \quad \text{(A28)}$$

REFERENCES

1. P. Sprangle, C. M. Tang, and I. B. Bernstein, *Phys. Rev. A* **28**, 2300 (1983).
2. W. T. Reid, in *Optimal Control and Differential Equations*, edited by A. B. Schwarzkopf, W. G. Kelley, and S. B. Eliason (Academic Press, New York, 1978), p. 189.
3. C. A. Swanson, *Comparison and Oscillation Theory of Linear Differential Equations* (Academic Press, London, 1968).

4. E. F. Mischenko and N. Kh. Rozov, *Differential Equations with Small Parameters and Relaxation Oscillations* (Plenum, New York, 1980).
5. K. E. Bullen and B. A. Bolt, *An Introduction to the Theory of Seismology*, 4th ed. (Cambridge Univ. Press, Cambridge, UK, 1985).
6. P. Ledoux and Th. Walraven, Variable stars, in *Handbuch der Physik, Vol. 51*, edited by S. Flügge (Springer-Verlag, Berlin, 1958), p. 353.
7. J. Heading, *An Introduction to Phase Integral Methods* (Methuen, London, 1962).
8. J. Kevorkian, *SIAM Rev.* **29**, 391 (1987).
9. J. Stoer and R. Bulirsch, *Introduction to Numerical Analysis* (Springer-Verlag, New York, 1983).
10. F. R. Gantmacher, *The Theory of Matrices*, Vol. 1 (Chelsea, New York, 1960), p. 72.
11. I. B. Bernstein, L. Brookshaw, and P. A. Fox, CSSR Technical Note [redacted] (unpublished).
12. J. P. Cox, *Theory of Stellar Pulsation* (Princeton Univ. Press, Princeton, 1980).
13. W. Unno *et al.*, *Non-radial Oscillations of Stars* (Tokyo Univ. Press, Tokyo, 1979).
14. T. G. Cowling, *Mon. Not. R. Astron. Soc.* **101**, 367 (1941).
15. S. Chandrasekhar, An Introduction to the Study of Stellar Structure (Dover, London, 1933).
16. Q. Chen, private communication (1989).
17. J. Christensen-Dalsgaard, Thesis, Cambridge University, 1977 (unpublished).
18. W. H. Press, B. P. Flannery, S. A. Teukolsky, and W. T. Vetterling, *Numerical Recipes* (Cambridge Univ. Press, Cambridge, UK, 1987).
19. D. J. Mullan and R. K. Ulrich, *Astrophys. J.* **331**, 1013 (1988).
20. S. Fishenko, M. Shkil, and L. Nikolenko, *Asymptotic Methods in the* [redacted] New York, 1967).